Materials Advances

ROYAL SOCIETY OF CHEMISTRY

PAPER

View Article Online
View Journal | View Issue

Cite this: *Mater. Adv.*, 2026, 7, 3362

Investigation of the adsorption nature of the hydroxyurea anti-cancer drug with pristine and transition metal (Co,Fe,Ni)-doped boron nitride fullerenes as a potential drug-delivery vehicle: a DFT study and COSMO analysis

Samiron Kumar Saha, *[a] Maliha Nishat, [a] Md. Rayhan Mostofa,[a] Md. Abul Hasnat,[b] Md. Atikur Rahman[a] and Md. Hafijur Rahman [a]

Finding an appropriate drug delivery vehicle for anti-cancer drugs is crucial to minimizing the adverse effects of chemotherapy and enhancing treatment efficacy. Among various approaches, nanostructure-based drug delivery systems have attracted significant attention. In this context, boron nitride ($B_{12}N_{12}$) nanocages have emerged as promising candidates for targeted drug delivery. In the present study, the adsorption behavior, reactivity, and electronic sensitivity of the hydroxyurea (HU) drug on $B_{12}N_{12}$, $CoB_{11}N_{12}$, $FeB_{11}N_{12}$, and $NiB_{11}N_{12}$ nanocages were investigated in both gas and aqueous media using first-principles density functional theory (DFT) calculations. Our findings indicate that all complexes are thermodynamically stable. The stability of these complexes in both media is confirmed by the increased negative adsorption energy (E_{AD}) and negative solvation energy of the doped nanocages. Among them, the HU/$NiB_{11}N_{12}$ complex exhibits the highest stability, with E_{AD} values of −1.00 eV (gas) and −0.86 eV (aqueous). Its stability is further supported by the enhanced dipole moment, increasing from 7.36 D to 11.40 D upon adsorption. Moreover, after adsorption, the HOMO–LUMO energy gap of the HU/$NiB_{11}N_{12}$ complex decreases significantly by ∼53.86% (gas) and ∼53.70% (aqueous), indicating substantial changes in its electronic properties. These results suggest that doped nanocages exhibit high sensitivity, making them excellent candidates for drug delivery applications. Quantum molecular descriptors further confirm that $NiB_{11}N_{12}$ offers higher sensitivity and reactivity compared to the other nanocages studied. Therefore, the HU/$NiB_{11}N_{12}$ complex stands out as the most promising drug delivery system, with $NiB_{11}N_{12}$ identified as the most effective nanocage carrier for the HU drug.

Received 6th November 2025,
Accepted 12th February 2026

DOI: 10.1039/d5ma01286d

rsc.li/materials-advances

1. Introduction

An anti-cancer drug delivery system is a technology designed to transport chemotherapeutic agents to specific target sites in the body and control their release, improving treatment effectiveness while reducing side effects. Cancer is a major cause of mortality worldwide and results from the uncontrolled growth of abnormal cells. Chemotherapy is commonly used to treat cancer,[1] and hydroxyurea (HU) is a non-alkylating antineoplastic drug[2–4] applied in several cancers and blood disorders.[5–12] However, its limited selectivity causes side effects such as gastrointestinal problems, bone marrow suppression, and skin reactions.[13]

Nanomedicine, which utilizes nanoparticle-mediated anti-cancer drug delivery to overcome the limitations of traditional anti-cancer drug administration, is largely responsible for this method of targeted anti-cancer drug delivery.[14] Anti-cancer drug carriers are designed as nanosized devices that offer a number of benefits for efficient anti-cancer drug delivery. This is why anti-cancer drug delivery and sensing applications are important fields for nanomaterials.

Recently, because of their high bioavailability, nanomaterials have drawn interest as drug vehicles to improve treatment efficacy and lessen negative effects.[15,16] Boron nitride (BN) nanomaterials have acquired heat resistance in air, outstanding structural and chemical stability, remarkable mechanical strength, a wide band gap, high reactivity, large surface areas, strong oxidation resistance, high thermal conductivity, fine

[a] *Department of Physics, Faculty of Science, Pabna University of Science and Technology, Pabna-6600, Bangladesh. E-mail: samiron@pust.ac.bd, malihanishat@pust.ac.bd, rayhanmostofa.180724@s.pust.ac.bd, atikphy@pust.ac.bd, mhrahman@pust.ac.bd*

[b] *Department of Physics, Faculty of Science, Jahangirnagar University, Dhaka-1342, Bangladesh. E-mail: hasnatarif92@gmail.com*

chemical inertness, *etc.*[17–20] Furthermore, the study by Chen *et al.* showed that because BN nanostructures don't cause harm, they can be used in biological applications.[21] Because of their exceptional physical, chemical, and surface characteristics, $B_{12}N_{12}$ nanoclusters are among the best BN nanoclusters for biosensors and biomedical applications.[22,23] Previous investigations have shown that the most stable structure is found in fullerene-like nanoclusters $X_{12}Y_{12}$ (Y = N, P, and X = B, Al).[24] The adsorption behavior of the metronidazole drug on boron carbide (BC), graphene, and $B_{12}N_{12}$ nanocages was investigated using DFT with the B3LYP/6-31G method.[25] The results revealed that BN nanocages exhibit higher sensitivity to the drug. Using DFT, Abdolahi *et al.* investigated the structural and electrical characteristics of the $B_{12}N_{12}$ nanocage functionalized with the drug celecoxib. They found that the $B_{12}N_{12}$ nanocage is a useful way to administer this drug.[26] Maliha Nishat *et al.* also investigated the interactions between clean and doped $B_{12}N_{12}$ nanocages and anagrelide drug molecules.[27] The adsorption nature of the miglitol (MT) anti-diabetic drug on the surface of gallium nitride (GNS), boron nitride (BNS), and boron carbide (BC3) nanosheets was examined using the DFT with B3LYP/6-31G technique. BNS and BC3 nanosheets were shown to be more sensitive to this drug.[28] The $X_{12}Y_{12}$ (X = B, Al and Y = N, P) nanocage has been examined as a possible vehicle for the MT drug using the DFT-D approach. The results showed that the $Al_{12}N_{12}$ nanocage is a useful drug delivery vehicle.[29] The adsorption behavior of the MT drug on the surfaces of $XB_{11}N_{12}$ nanocages (where X stands for Ga, In, and Al) and $B_{12}N_{12}$ has been investigated. It has been found that the MT drug is better transported *via* MT/$AlB_{11}N_{12}$ and MT/$GaB_{11}N_{12}$ nanocages.[30] DFT has recently been used to study the electrical characteristics and adsorption behavior of HU on pure and carbon-doped $B_{24}N_{24}$ nanocages.[31]

In this first-principles study, we examined the potential of $B_{12}N_{12}$ nanocages as drug delivery vehicles for the HU drug using DFT. To enhance the adsorption properties, elemental modifications were introduced by doping with Co, Fe, and Ni atoms, leading to the construction of $CoB_{11}N_{12}$, $FeB_{11}N_{12}$, and $NiB_{11}N_{12}$ nanocages, respectively, for comparative analysis. The adsorption behavior of the HU drug on these nanocages was evaluated in both gas and aqueous media. To gain deeper insights, we analyzed the electron density (ED), interaction distances, electrostatic potential (ESP), and adsorption energies (E_{AD}). Additionally, the density of states (DOS) and energy gap variations were studied to explore the electronic behavior. The work function (φ) and quantum molecular descriptors (QMD) were calculated to assess the reactivity of the nanocages toward the HU drug. Finally, to evaluate the effect of solvent interactions, surface analysis was performed using the conductor-like screening model (COSMO).

2. Computational details

The purpose of this research is to deepen the knowledge of the adsorption behavior of the HU anticancer drug on the surface of nanostructures, transition metal-doped boron nitride fullerenes, using a theoretical approach called first-principles simulation. Using the DFT framework's output from the DMol3 module, the geometry optimization of the HU drug's adsorption capability on the $B_{12}N_{12}$, $CoB_{11}N_{12}$, $FeB_{11}N_{12}$, and $NiB_{11}N_{12}$ nanocages in both phases was examined. The generalized gradient approximation (GGA) was used to optimize the structures under investigation.[32] The exchange–correlation connection was described using the GGA Perdew–Burke–Ernzerhof (PBE) functional. Grimme's dispersion correction (DFT-D) methods were used in all calculations to account for the long-range electron effect. A double numerical basis set plus polarization (DNP) and DFT semi-core pseudopotentials have been used for the core treatment.[33] It is demonstrated that the basis set superposition error (BSSE) can be reduced by using the DNP basis set built in DMol3.[34] Optimization of the geometry has been done under spin-unrestricted conditions. To increase computational accuracy in all investigations, the following parameters were set: smearing point, maximum displacement, energy tolerance, electronic SCF convergence, maximum force, and real-space global cut-off diameter: 5 mHa, 5 mÅ, 20 μHa, 10 μeV, 4 mHa $Å^{-1}$, and 2.5 Å, respectively. These figures are similar to those from our previous investigation.[29,30]

The following equations were used to calculate the energy gap (E_g), adsorption energy (E_{AD}), band gap difference in percentage (%ΔE_g), hardness (η), chemical potential (μ), softness (S), and electrophilicity (ω) for both media.[29,30]

Energy gap:

$$E_g = E_L - E_H \quad (1)$$

where E_L and E_H represent the energy of the LUMO and HOMO levels, respectively.

Adsorption energy:

$$E_{AD} = E_{complex} - E_{HU} - E_{nanocages} \quad (2)$$

where $E_{nanocages}$, E_{HU}, and $E_{complex}$ denote the total energies of the nanocages, HU drug, and drug–nanocage complex, respectively.

The band gap difference in percentage:

$$\%\Delta E_g = \frac{E_{g1} - E_{g2}}{E_{g2}} \times 100\% \quad (3)$$

where E_{g1} and E_{g2} represent the band gaps of the complex compound and absorbent nanocage, respectively.

$$\eta = \frac{E_L - E_H}{2} \quad (4)$$

$$\mu = -\frac{E_H + E_L}{2} \quad (5)$$

$$S = \frac{1}{2\eta} \quad (6)$$

$$\omega = \frac{\mu^2}{2\eta} \quad (7)$$

We calculated the vibrational modes of our complexes and adsorbent nanocages to verify that the systems correspond to

real local minima. Considering that water constitutes the majority of the human body, the adsorption behavior of the HU drug on nanocage surfaces was further investigated in an aqueous medium (dielectric constant = 78.54) using the COSMO method.[16,35] All the aforementioned parameters were then recalculated in water using the same theoretical framework.

3. Results and discussion

3.1 Geometric configurations

In both stages, we optimize our estimated adsorbent nanocages ($B_{12}N_{12}$, $CoB_{11}N_{12}$, $FeB_{11}N_{12}$, and $NiB_{11}N_{12}$). The optimized structures are shown in Fig. 1 along with the ESP maps, ED, and HOMO–LUMO. Because it contains both tetragonal and hexagonal rings with B–N connections, the $B_{12}N_{12}$ nanocage has initially been seized.[27,36] The $B_{12}N_{12}$ structure contains two types of non-equivalent B–N bonds: one with a length of 1.44 Å formed between two atoms in a hexagonal ring, and another with a length of 1.49 Å formed between atoms connecting a hexagonal ring to a tetragonal ring. These bond lengths and the previous theoretical analysis are fairly comparable.[27,37–39] Co, Fe, and Ni atoms are replaced with one boron (B) atom in $B_{12}N_{12}$, resulting in $CoB_{11}N_{12}$, $FeB_{11}N_{12}$, and $NiB_{11}N_{12}$ nanocages, respectively, for comparison of their adsorption behaviors. The studied nanocages maintain a planar phase, with only minor variations in the B–N bond length, E_L, and E_H. To ensure structural stability, the B–N bond lengths in both hexagonal and tetragonal units remain nearly unchanged. In the doped systems, the Co–N, Fe–N, and Ni–N bond lengths are 1.823 Å in the hexagonal sites and 1.861 Å in the tetragonal sites, consistent with previous reports.[39,40] The slight increase in bond lengths at the doping sites contributes to stabilizing the atomic arrangements of these nanocages. Frontier molecular orbital (FMO) analysis was performed to investigate the electronic structure. The HOMO orbitals are primarily localized on the N atoms on the right side of the nanocages, whereas the LUMO orbitals are concentrated on the dopant atoms (Co, Fe, and Ni) and the B atoms on the left side. The HOMO–LUMO energy gap (E_g) was calculated to be 5.08 eV for $B_{12}N_{12}$, 1.13 eV for $CoB_{11}N_{12}$, 0.53 eV for $FeB_{11}N_{12}$, and 0.47 eV for $NiB_{11}N_{12}$. Substitution of Co, Fe, and Ni for B atoms significantly decreases the energy gap, following the trend: $B_{12}N_{12} > CoB_{11}N_{12} > FeB_{11}N_{12} > NiB_{11}N_{12}$ (Table 1). The electron density (ED) and electrostatic potential (ESP) maps (Fig. 1m–p and q–t) further illustrate charge distribution. Blue regions indicate positive ion zones, while yellow regions indicate negative ion zones. Negative charges are mainly localized around the electron-rich N atoms, whereas positive charges are concentrated around the B, Co, Fe, and Ni atoms due to their electron-deficient nature. To confirm configurational stability, vibrational mode calculations were carried out under infrared radiation. Table 2 presents the minimum and maximum vibrational frequencies for each system. Since all frequencies are positive, the structures are confirmed to be stable and suitable for experimental synthesis. The vibrational frequencies for $B_{12}N_{12}$, $CoB_{11}N_{12}$, $FeB_{11}N_{12}$, and $NiB_{11}N_{12}$ were found to lie in the ranges of 312.7–1407.8 cm^{-1}, 184.5–1415.2 cm^{-1}, 161.4–1414.3 cm^{-1}, and 105.4–1408.5 cm^{-1}, respectively. For the HU/nanocage complexes, the vibrational frequencies were observed as follows: 8.6–3638.6 cm^{-1} for HU/$B_{12}N_{12}$, 35.9–3640.7 cm^{-1} for HU/$CoB_{11}N_{12}$, 12.3–3633.3 cm^{-1} for HU/$FeB_{11}N_{12}$, and 15.0–3637.4 cm^{-1} for HU/$NiB_{11}N_{12}$. These results confirm that each customized adsorbent and its corresponding complex represent a true local minimum and phase-stable system.

Fig. 2 presents the ESP maps and HOMO–LUMO distributions of the HU drug in both optimized and relaxed configurations. As illustrated, the HU molecules possess two electrophilic and two nucleophilic sites. The calculated bond angles (δ) of the HU drug are as follows: H–O–N (109.470°), O–N–H (104.480°), H–N–C (104.480°), O–N–C (120.010°), N–C–N (119.990°), C–N–H (120.010°), H–N–H (109.050°), N–C–O (109.470°), and C–O–N (124.680°). The corresponding bond lengths are: O–C (1.54 Å), H–N (1.00 Å), C–N (1.54 Å), O–N (1.54 Å), and H–O (0.96 Å).

The LUMO levels of the O–C bond, N atoms, and H–O bond are set at −0.59 eV in the gas phase and −5.66 eV, and −0.48 eV in the water medium, whereas the HOMO level of HU for the C and O atoms is set at −5.54 eV. Positive ions are localized in the O–C–H region, while negative ions are concentrated in the N atom region, as seen in the ESP map of HU.

3.2 The HU drug's adsorption onto the absorbent nanocages

The chemical structure of the HU drug consists of four types of atoms: C, N, H, and O. To study the adsorption nature of the HU drug, we investigated its interaction with nanocages, leading to various possible complex configurations. Among these, the best adsorption arrangement was determined to be the lowest-energy complex, and further analysis was carried out using these systems. According to our calculations, the lowest-energy complex structure is formed when we add our dopant onto the top side of our investigated nanostructure. So, all our calculations and further analysis were carried out by using these types of complex structures. For all complexes, the global minima were achieved in both phases. The gas-phase optimized structures and their respective adsorption distances are shown in Fig. 3. The observation of negative E_{AD} for all complexes indicates a favorable interaction between the HU drug and nanocages.[41] We analyzed the values of E_{AD} for each complex in both phases. The values are all negative, which affirms the complexes' stability and attractive interaction behavior.[29,41] The HU drug is adsorbed with −0.98, −0.99, −0.57, and −1.00 eV energy at a distance of 1.67 Å, 1.69 Å, 1.69 Å, and 1.67 Å, in the gas medium and −0.96, −0.93, −0.41, and −0.86 energy at a distance of 1.62 Å, 1.63 Å, 1.64 Å, and 1.63 Å in the aqueous medium for the $B_{12}N_{12}$, $CoB_{11}N_{12}$, $FeB_{11}N_{12}$, and $NiB_{11}N_{12}$ nanocages, respectively (Table 2). Consequently, there is an inverse relationship between the E_{AD} and the minimum distance between the HU drug and the studied nanocages.

Table 2 presents the E_{AD} values calculated before and after the adsorption of the HU drug on $B_{12}N_{12}$, $CoB_{11}N_{12}$, $FeB_{11}N_{12}$, and $NiB_{11}N_{12}$ nanocages. The variation in E_{AD} indicates

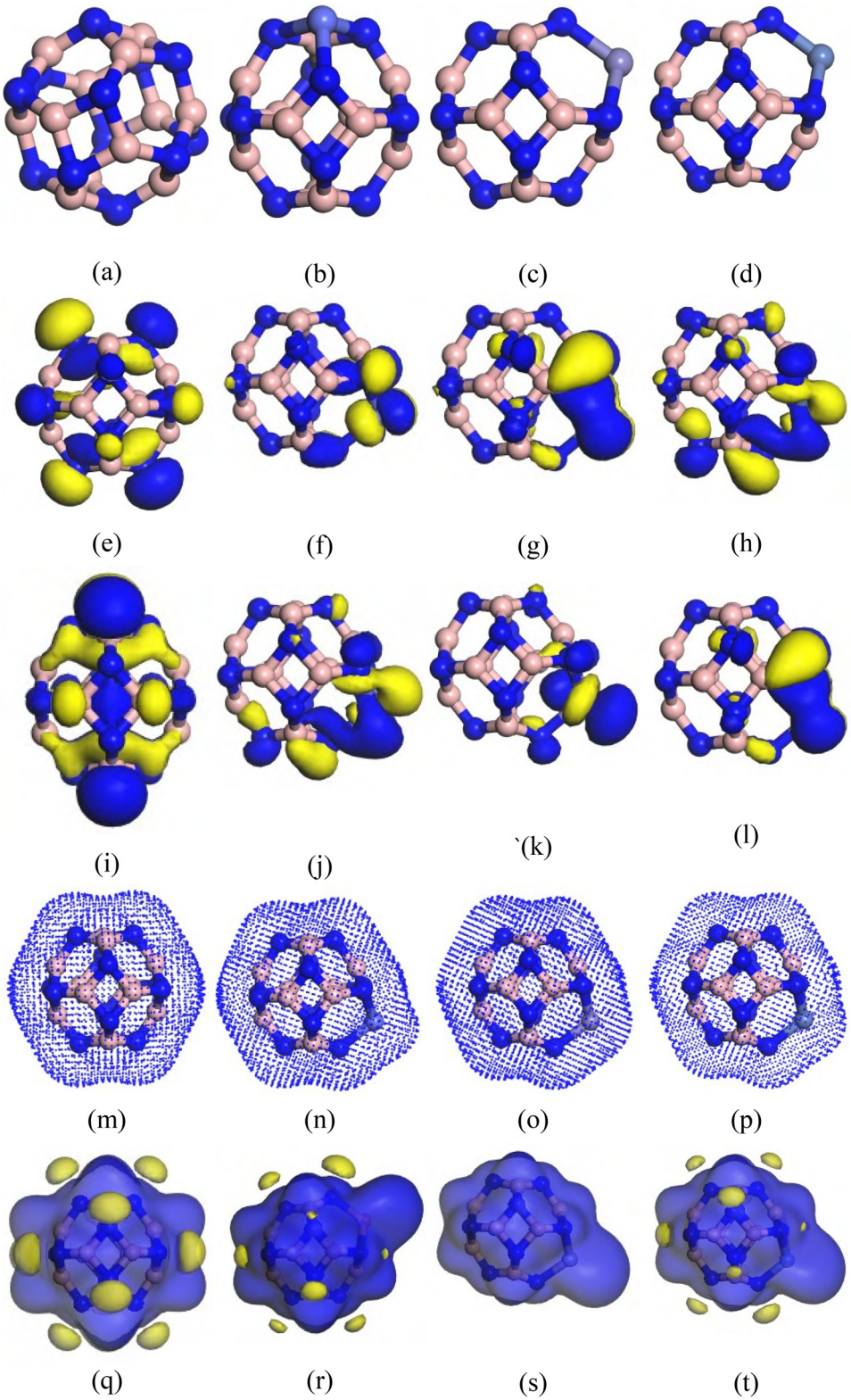

Fig. 1 (a)–(d) Optimized structures, (e)–(h) HOMO, (i)–(l) LUMO, (m)–(p) ED, and (q)–(t) ESP maps of the $B_{12}N_{12}$, $CoB_{11}N_{12}$, $FeB_{11}N_{12}$, and $NiB_{11}N_{12}$ nanocages, respectively. Atoms are color-coded as follows: nitrogen (N) (blue), boron (B) (peach), cobalt (Co) (light blue), iron (Fe) (silver grey), and nickel (Ni) (silver white).

Table 1 The HOMO energy (E_H), LUMO energy (E_L), and HOMO–LUMO energy gap (E_g) in eV, along with the percentage change in the HOMO–LUMO energy gap (%ΔE_g), were assessed for the examined adsorbent nanocages, HU drug, and drug–nanocage complexes in both phases

	Gas phase				Water phase			
Structures	E_H	E_L	E_g	%ΔE_g	E_H	E_L	E_g	%ΔE_g
HU Drug	−5.54	−0.59	4.95	—	−5.66	−0.48	5.18	—
$B_{12}N_{12}$	−7.04	−1.96	5.08	6.60	−7.06	−1.89	5.17	3.71
HU/$B_{12}N_{12}$	−6.35	−1.61	4.74		−6.55	−1.56	4.98	
$CoB_{11}N_{12}$	−5.79	−4.66	1.13	1.71	−5.69	−4.55	1.13	1.80
HU/$CoB_{11}N_{12}$	−5.33	−4.22	1.11		−5.45	−4.33	1.11	
$FeB_{11}N_{12}$	−5.72	−5.19	0.53	53.80	−5.74	−5.08	0.66	43.21
HU/$FeB_{11}N_{12}$	−4.89	−3.74	1.15		−4.98	−3.82	1.16	
$NiB_{11}N_{12}$	−5.89	−5.42	0.47	53.86	−5.88	−5.66	0.49	53.70
HU/$NiB_{11}N_{12}$	−5.99	−4.97	1.02		−6.18	−5.39	1.05	

noticeable interaction between the HU molecule and the investigated nanocages. The relatively small adsorption distance (d) further confirms a strong affinity between the drug and the carrier surface. Generally, an increase in E_{AD} corresponds to a reduction in the adsorption distance, suggesting enhanced interaction strength. Our findings therefore support improved adsorption behavior, consistent with previously reported studies. However, adsorption is not governed solely by E_{AD}. Orbital interactions also play a crucial role in determining the stability and strength of the drug–nanocage complexes. These effects were thoroughly examined in our earlier discussion of HOMO–LUMO energy levels and electronic distribution characteristics. The calculated E_{AD} values are summarized in Table 2. Based on their magnitudes, the studied complexes predominantly exhibit physisorption behavior.[42] As a result, the HU anticancer drug is expected to be released relatively easily from the nanocage surface, which may be advantageous for controlled drug delivery applications.[29]

Lastly, the E_{AD} suggests that our investigated nanocages have an equally potent potential to deliver the HU drug. Among them, the HU/$NiB_{11}N_{12}$ nanocage shows superior performance, as it possesses the highest E_{AD} value (Table 2), making it the best possible structure. The interaction distance (d) is used to determine E_{AD}. The LUMO and HOMO orbital analysis shows how their electronic configurations vary during interaction. The sensing capacities of $B_{12}N_{12}$, $CoB_{11}N_{12}$, $FeB_{11}N_{12}$, and $NiB_{11}N_{12}$ nanocages are demonstrated by the variations in their electrical properties upon interaction with the HU anti-cancer drug. The %ΔE_g and E_g data are tabulated in Table 1, which are assessed and shown in Fig. 3, to investigate the sensitivity of the $B_{12}N_{12}$, $CoB_{11}N_{12}$, $FeB_{11}N_{12}$, and $NiB_{11}N_{12}$ nanocages towards the HU drug using frontier molecular orbital (FMO) analysis (LUMO and HOMO).

Furthermore, the E_g trend is displayed in Fig. 4 both before and after the adsorption of the HU drug onto the nanocages. In all studied complexes, the HOMO is mainly localized on the HU drug molecules, whereas the LUMO is primarily found on the adsorbent nanocages. After adsorption, both E_H and E_L values of HU/$B_{12}N_{12}$, HU/$CoB_{11}N_{12}$, HU/$FeB_{11}N_{12}$, and HU/$NiB_{11}N_{12}$ nanocages become stabilized. In the gas medium, the E_H values of HU/$B_{12}N_{12}$, HU/$CoB_{11}N_{12}$, HU/$FeB_{11}N_{12}$, and HU/$NiB_{11}N_{12}$

Table 2 The estimated interaction distance (d, in Å) between the HU drug and the studied nanocages, dipole moment (DM, in Debye), adsorption energy (E_{AD}, in eV), and low and high vibrational frequencies (ν_{low} and ν_{high}, in cm^{-1})

	Gas phase					Water phase				
Structures	d	DM	E_{AD}	ν_{low}	ν_{high}	d	DM	E_{AD}	ν_{low}	ν_{high}
HU drug	—		—	188.8	3629.1	—		—	180.2	3628.3
$B_{12}N_{12}$		0.00	−0.98	312.7	1407.8		0.00	−0.96	311.6	1387.9
HU/$B_{12}N_{12}$	1.67	7.03		8.6	3638.6	1.62	10.72		0.0	3622.2
$CoB_{11}N_{12}$		2.00	−0.99	184.5	1415.2		3.65	−0.93	187.1	1393.3
HU/$CoB_{11}N_{12}$	1.69	7.20		35.9	3640.7	1.63	11.56		34.4	3614.3
$FeB_{11}N_{12}$		3.03	−0.57	161.4	1414.3		5.42	−0.41	169.6	1386.9
HU/$FeB_{11}N_{12}$	1.69	7.29		12.3	3633.3	1.64	11.47		17.4	3617.6
$NiB_{11}N_{12}$		1.58	−1.00	105.4	1408.5		2.79	−0.86	110.5	1382.8
HU/$NiB_{11}N_{12}$	1.67	7.36		15.0	3637.4	1.63	11.40		0.0	3609.0

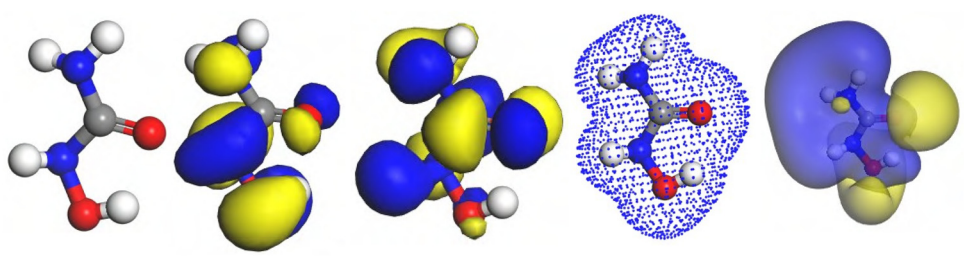

(a) (b) (c) (d) (e)

Fig. 2 The optimized structure of the HU drug, along with its HOMO, LUMO, ED, and ESP maps, are shown in (a), (b), (c), (d), and (e), respectively. The following color codes are used for the atoms: red stands for O, blue for N, white for H, and ash for C.

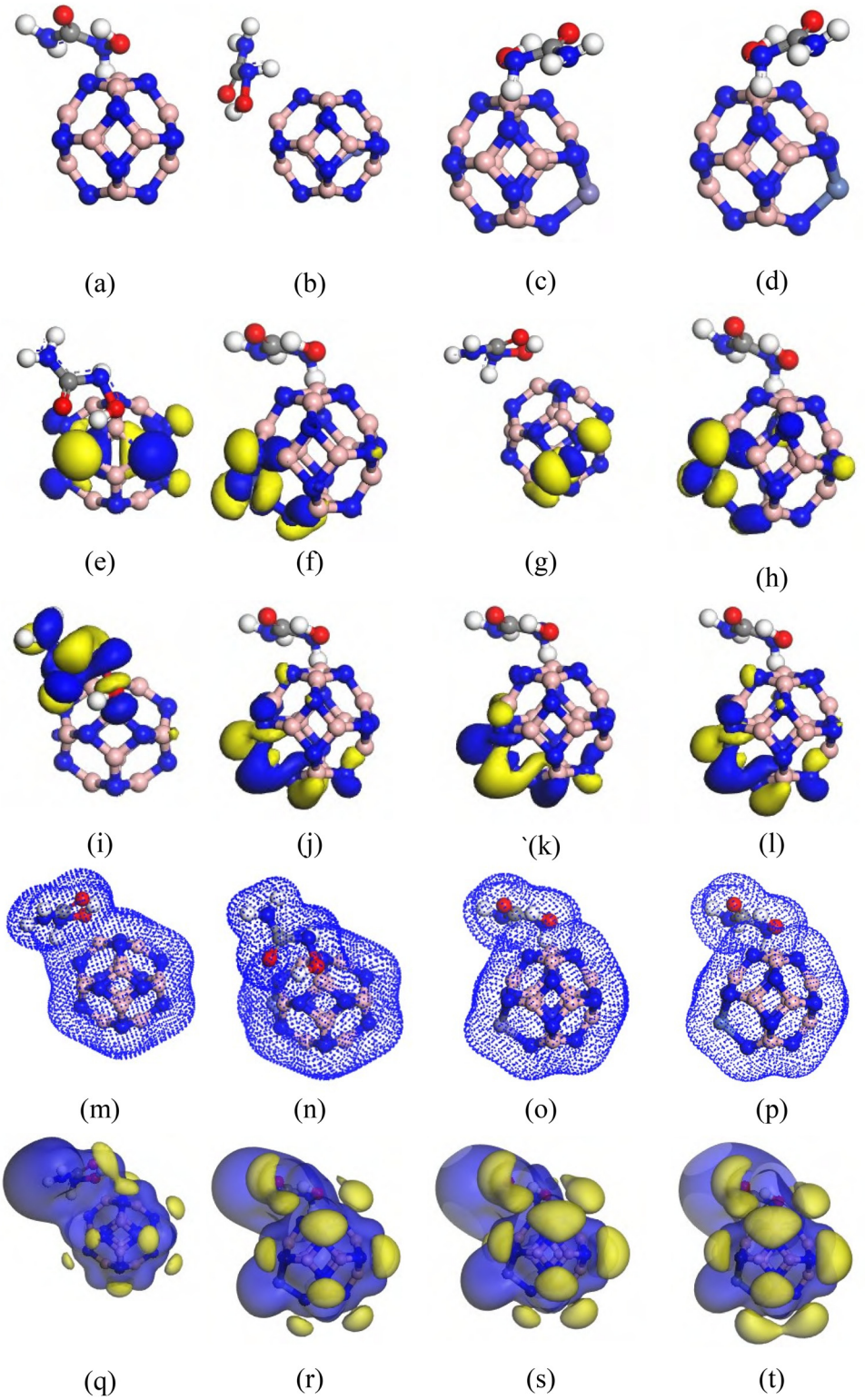

Fig. 3 At the same theoretical level in the gas phase, the results include (a)–(d) optimal configurations, (e)–(h) HOMO orbitals, (i)–(l) LUMO orbitals, (m)–(p) electron density (ED), and (q)–(t) electrostatic potential (ESP) maps of the complex compounds, respectively.

nanocages are −6.35 eV, −5.33 eV, −4.89 eV, and −5.99 eV, while their corresponding E_L values are −1.61 eV, −4.22 eV, −3.74 eV, and −4.97 eV, respectively. Consequently, the calculated E_g values are 4.74 eV for HU/$B_{12}N_{12}$, 1.11 eV for HU/$CoB_{11}N_{12}$, 1.15 eV for HU/$FeB_{11}N_{12}$, and 1.02 eV for HU/$NiB_{11}N_{12}$, with the respective $\%\Delta E_g$ values being about 6.60%, 1.71%, 53.80%, and 53.86% in the gas medium. Similar calculations were performed in the water phase, and the results

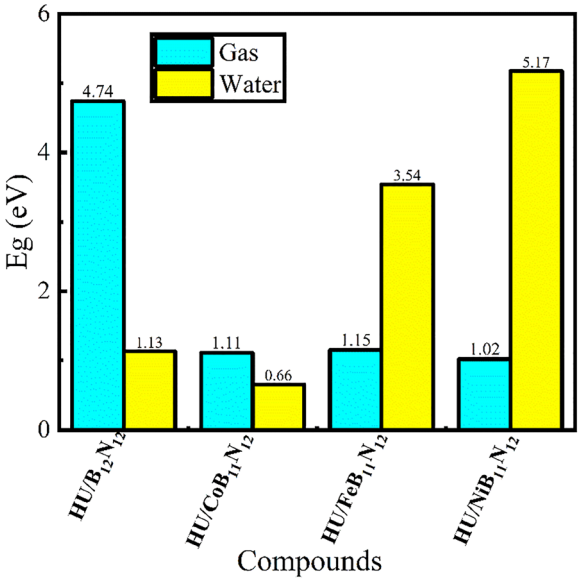

Fig. 4 The trend of the HOMO–LUMO energy gap (E_g) of the investigated complexes in both media.

are presented in Table 1. The highest adsorption energy (E_{AD}) is observed for the $HU/NiB_{11}N_{12}$ complex, reaching −1.00 eV when the drug molecules adsorb at a distance of 1.67 Å. Overall, the $\%\Delta E_g$ values of the $B_{12}N_{12}$, $CoB_{11}N_{12}$, $FeB_{11}N_{12}$, and $NiB_{11}N_{12}$ nanocages decrease significantly, ranging from about 53.86% to 1.71% in the gas phase and from about 53.70% to 1.80% in the water phase after HU drug adsorption.

The E_g is displayed as a bar graph in Fig. 4. Higher molecular polarizability, which often indicates increased chemical reactivity and decreased kinetic stability, is correlated with a lower E_g value.[43] Additionally, the following formula demonstrates how the conduction electron population (N) affects E_g.[27,44]

$$N = AT^{\frac{2}{3}} \exp\left(\frac{E_g}{kT}\right) \quad (8)$$

where k denotes the Boltzmann constant and A (electrons per m^3 per $k^{3/2}$) is a constant.[45] Eqn (8) states that greater electrical conductivity, which can be transformed into an electrical signal for drug identification, is the result of a lower E_g value.

One of the most important parameters for drug distribution applications is the energy gap (E_g) value. The density of states (DOS) spectra, shown in Fig. 5, can be used to investigate the shift in E_g further. Fig. 5 displays the DOS spectra of the $B_{12}N_{12}$, $CoB_{11}N_{12}$, $FeB_{11}N_{12}$, and $NiB_{11}N_{12}$ nanocages, both before and during HU drug adsorption. After adsorption, an additional phase appears near the Fermi level, leading to a reduction in E_g. The number of conduction electrons is increased by this reduction, which is essential for the planned drug delivery mechanism. Notably, HU adsorption decreases E_g for all nanocages except $NiB_{11}N_{12}$, whereas E_g increases instead. These band gap variations, also reflected in the DOS spectra (Fig. 5), arise from the fluctuations of the HOMO and LUMO states following HU adsorption.

3.3 Dipole moment analysis

One essential property of molecules or complexes that shows the asymmetric charge distribution between them is the dipole moment (DM).[46] It is a crucial metric for analyzing complex or molecular symmetry.[25,37] Greater ion transfer and a more robust interaction between HU and the nanocages are indicated by a higher DM value. The DM for $B_{12}N_{12}$ was determined to be 0.00 Debye (D), indicating that there is no ion separation between the atoms.[47] The DM values of $CoB_{11}N_{12}$, $FeB_{11}N_{12}$, and $NiB_{11}N_{12}$ were found to be 2.00 D, 3.03 D, and 1.58 D, respectively, which are consistent with the previous studies.[27,39] After the adsorption of the HU drug onto these nanocages, the DM values increased in both phases compared to the pure nanocages. Specifically, the DM values for the complexes $HU/B_{12}N_{12}$, $HU/CoB_{11}N_{12}$, $HU/FeB_{11}N_{12}$, and $HU/NiB_{11}N_{12}$ were observed to be 7.03 D, 7.20 D, 7.29 D, and 7.36 D, respectively. These results are summarized in Table 2. Thus, $HU/B_{12}N_{12} > HU/CoB_{11}N_{12} > HU/FeB_{11}N_{12} > HU/NiB_{11}N_{12}$ is the ascending order of the DM. The DM of complexes and nanocages is much higher in the aqueous medium than it is in the gas medium. For the $HU/B_{12}N_{12}$, $HU/CoB_{11}N_{12}$, $HU/FeB_{11}N_{12}$, and $HU/NiB_{11}N_{12}$ nanocages, the DM was seen at around 10.72 D, 11.56 D, 11.47 D, and 11.40 D, respectively. Consequently, these findings suggest that the responsiveness of the HU rises with an increase in the DM. The determined DMs demonstrate that the polarity of the complex nanostructures is greater in the aqueous phase. Importantly, the DM also accounts for the water solubility of the complexes, making them highly suitable for biological drug delivery. The $HU/NiB_{11}N_{12}$ complex is an excellent choice for drug delivery applications since it shows the highest DM value in both the gas and aqueous phases. Greater solubility in the aqueous phase is indicated by a higher DM value.

3.4 Quantum molecular descriptor (QMD) analysis

Quantum molecular descriptors (QMDs), including chemical potential (μ), global hardness (η), global softness (S), and electrophilicity index (ω), were used to assess the stability and reactivity of the complexes (Table 3). A decrease in μ generally corresponds to enhanced stability and reduced reactivity, whereas a higher μ indicates the opposite.[48] Upon HU adsorption, μ decreases for all systems, implying improved structural stability. Higher η reflects greater resistance to electronic deformation[49] and lower reactivity, while increased S and ω indicate enhanced reactivity.[50] Our results show a general decrease in η accompanied by increases in S and ω after HU adsorption, except for the $HU/NiB_{11}N_{12}$ complex, which exhibits increased η and reduced S and ω, suggesting superior chemical stability but lower reactivity. Overall, HU adsorption significantly alters the stability–reactivity balance of the investigated nanocages.

3.5 Work function analysis

The sensitivity of the HU drug to the nanocages is expressed mathematically by the work function (φ). Thus, we investigated how the HU drug altered the nanocages' φ. It is possible to use

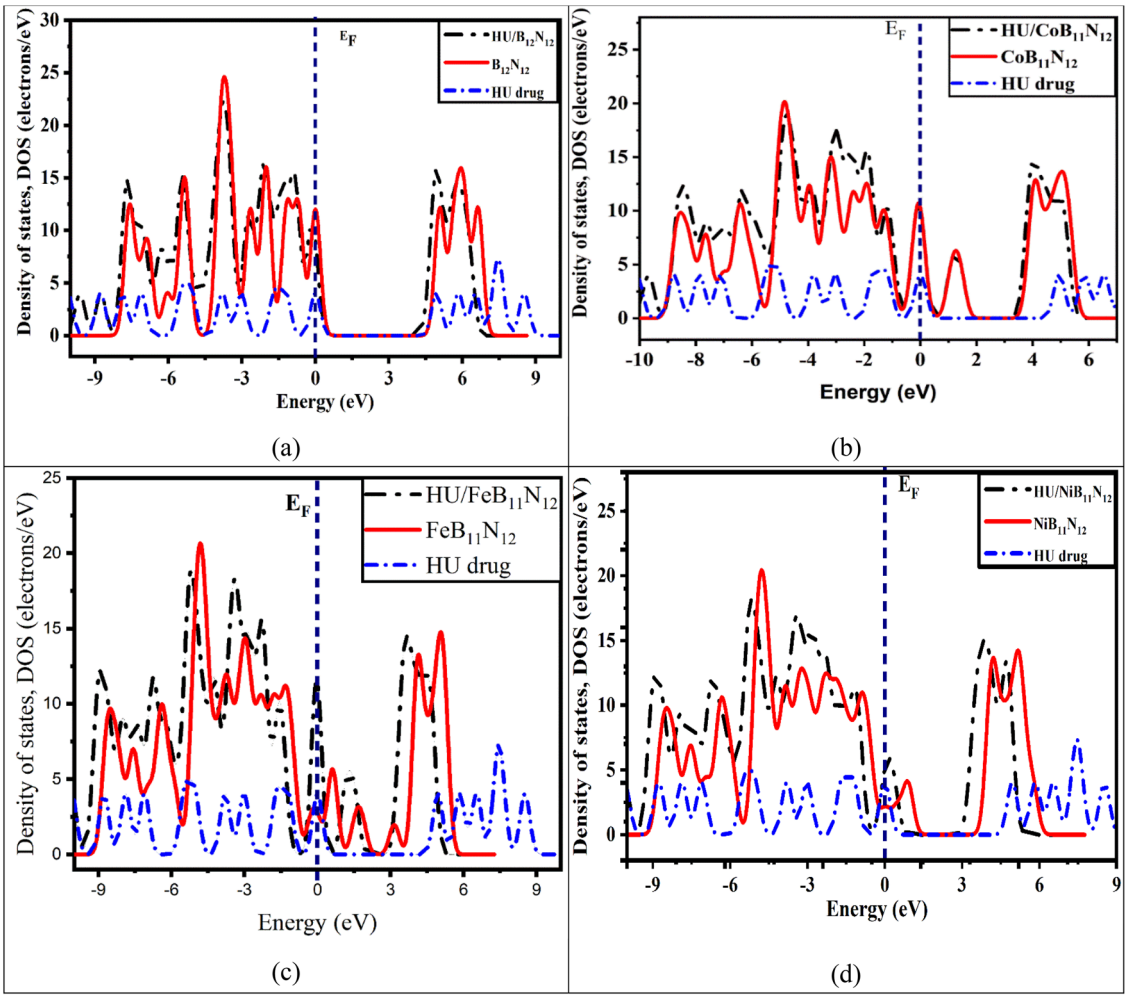

Fig. 5 Total DOS for (a) $B_{12}N_{12}$, (b) $CoB_{11}N_{12}$, (c) $FeB_{11}N_{12}$, and (d) $NiB_{11}N_{12}$ nanocages before and after the HU drug was adsorbed. The dotted line represents the Fermi energy (E_F).

the equation to find the minimum energy needed to extract one electron from the Fermi level to infinity.[51]

$$\varphi = V_{el(+\infty)} - E_F \quad (9)$$

E_F represents the Fermi level, while the electrostatic potential of an electron at infinity, $V_{el(+\infty)}$, is taken as zero, *i.e.*, $V_{el(+\infty)} = 0$, distant from the surface. Therefore, $\varphi = -E_F$. The main mechanism is that after the HU drug is adsorbed, the adsorbent's field emission characteristics are changed by the change in φ; when the gate voltage is commuted, an electrical signal is generated.[52] The change in φ upon drug adsorption was determined using estimations from

$$\Delta\varphi = \frac{\varphi_b - \varphi_a}{\varphi_b} \times 100\% \quad (10)$$

where the work functions, φ_a and φ_b are those that occur before and after the adsorption of the HU drug on the nanocages, respectively.

The computed values of φ are presented in Table 4, and Fig. 6 illustrates the variation of φ after the adsorption process. Two significant metrics, E_F and φ, increase after the HU drug is adsorbed onto the nanocage's surface in gas as well as water medium, except for $HU/NiB_{11}N_{12}$. The values of φ are significantly altered when the HU drug adsorbs onto our predicted nanocages. The negative value of $\Delta\varphi$ denotes an increase in φ,

Table 3 For the systems under study in both media, the computed values of the chemical potential (μ), global softness (S) (in eV^{-1}), global hardness (η), and electrophilicity index (ω) (in eV) are presented

	Gas phase				Water phase			
Structures	μ	S	η	ω	μ	S	η	ω
HU drug	4.50	0.20	2.54	3.99	3.07	0.19	2.59	1.82
$B_{12}N_{12}$	3.98	0.21	2.37	3.35	4.47	0.19	2.59	3.87
$HU/B_{12}N_{12}$	5.22	0.89	0.56	24.21	4.06	0.20	2.49	3.30
$CoB_{11}N_{12}$	4.78	0.90	0.55	20.60	5.12	0.88	0.57	23.12
$HU/CoB_{11}N_{12}$	5.46	1.89	0.27	56.15	4.89	0.90	0.56	21.48
$FeB_{11}N_{12}$	4.31	0.87	0.57	16.20	5.41	1.52	0.33	44.51
$HU/FeB_{11}N_{12}$	4.73	0.31	1.62	6.92	4.40	0.86	0.58	16.73
$NiB_{11}N_{12}$	5.48	0.98	0.51	29.52	5.63	2.06	0.24	65.34
$HU/NiB_{11}N_{12}$	4.50	0.20	2.54	3.99	5.66	0.95	0.52	30.53

Table 4 The systems under research in gas and water media are listed together with their Fermi level (E_F), work function (φ) in eV, and φ change (%$\Delta\varphi$)

	Gas phase			Water phase		
Structures	E_F	φ	%$\Delta\varphi$	E_F	φ	%$\Delta\varphi$
HU drug	−3.06	3.06	—	−3.07	3.07	—
$B_{12}N_{12}$	−4.50	4.50	11.42	−4.47	4.47	9.36
HU/$B_{12}N_{12}$	−3.98	3.98		−4.06	4.06	
$CoB_{11}N_{12}$	−5.22	5.22	8.56	−5.12	5.12	4.50
HU/$CoB_{11}N_{12}$	−4.78	4.78		−4.89	4.89	
$FeB_{11}N_{12}$	−5.46	5.46	20.97	−5.41	5.41	18.65
HU/$FeB_{11}N_{12}$	−4.31	4.31		−4.40	4.40	
$NiB_{11}N_{12}$	−5.66	5.66	3.08	−5.63	5.63	0.44
HU/$NiB_{11}N_{12}$	−5.48	5.48		−5.66	5.66	

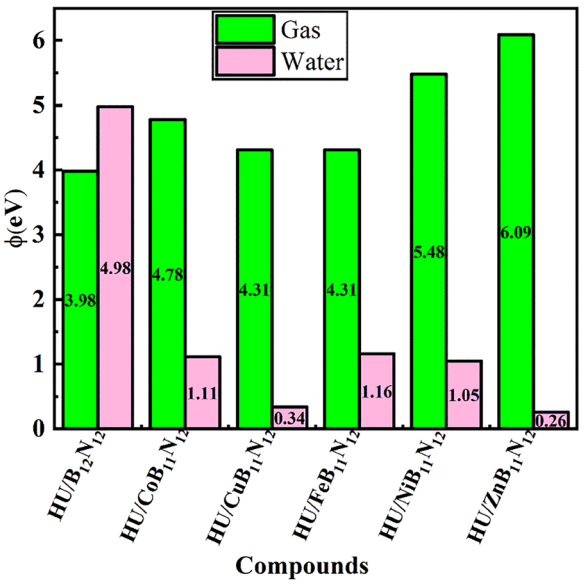

Fig. 6 A diagram showing the variation of φ when the HU drug is adsorbed onto the nanocages.

whereas the positive sign denotes a decrease after the adsorption of the HU drug.

The values of φ are significantly altered when the HU medication adsorbs onto our anticipated nanocages. φ enhances absorption by fortifying the electrostatic attraction to negatively charged cell membranes. Reducing φ (to more neutral or negative) increases biocompatibility and circulation time. Therefore, φ modulation is a technique for developing responsive or customized drug delivery systems. Following the adsorption of the HU drug onto the HU/$B_{12}N_{12}$, HU/$CoB_{11}N_{12}$, HU/$FeB_{11}N_{12}$, and HU/$NiB_{11}N_{12}$ nanocages, φ increases by approximately 11.42%, 8.56%, 28.31%, 20.97%, 3.08%, and 22.30% in the gas medium, respectively, while a decrease of about 3.08% was observed for HU/$NiB_{11}N_{12}$. Notably, HU/$NiB_{11}N_{12}$ exhibited relatively high φ values in both media, highlighting its potential as an efficient carrier for HU drug delivery. Additionally, the values of φ increased in the aqueous phase, indicating larger sensitivity.

3.6 COSMO surface study

When the complexes are observed in a living organism, they may be encased in water molecules. Therefore, examining the effects of the solvent phase on anti-cancer drug distribution is crucial. The impact of the solvent on the HU drug's adsorption properties on the nanocages, resulting in modifications to its electronic behavior, was examined in our previous sections. To gain better insights into the polarities of the complexes and the effects of the solvent phase, the surfaces of COSMO have been examined.

We conducted a COSMO surface study of our compounds to learn more about the solvent effect. The polar and non-polar portions of the complexes are illustrated on the COSMO surfaces as shown in Fig. 7. The positively charged region on this COSMO surface is shown by the red part, which denotes a hydrogen bond donor (HBD) region. The complexes' negatively charged hydrogen bond acceptor (HBA) region, on the other hand, is shown by the blue section.[41,53] The yellowish-green part also points to a non-polar, neutral area of the complexes. Our study revealed that the HBD region grew after the HU was adsorbed on the nanocages, particularly on the HU/$NiB_{11}N_{12}$,

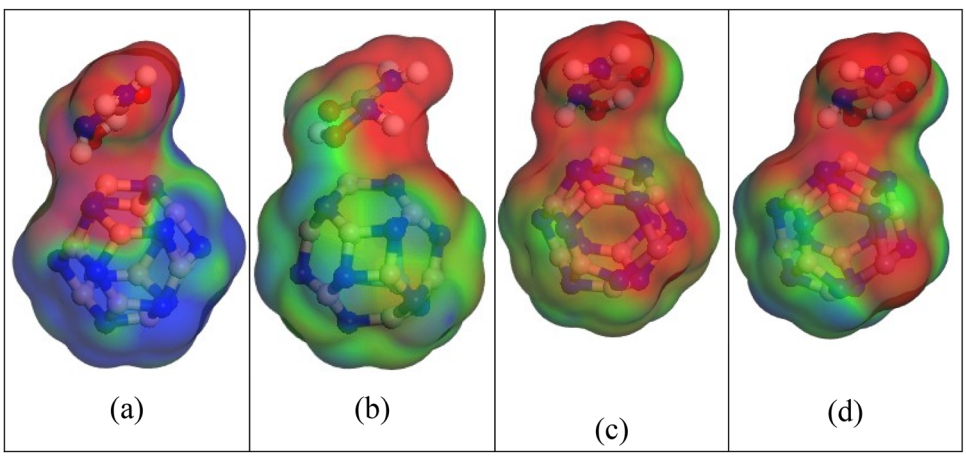

Fig. 7 The comparable COSMO surfaces are displayed for (a) HU/$B_{12}N_{12}$, (b) HU/$CoB_{11}N_{12}$, (c) HU/$FeB_{11}N_{12}$, and (e) HU/$NiB_{11}N_{12}$.

suggesting that the complexes in the aqueous solvent medium were highly polar. According to our DM measurement, the polarity of the complexes in the solvent phase was greatly enhanced by the adsorption of the HU drug molecules on the nanocages.

4. Conclusions

Using DFT calculations in both gas and aqueous phases, the adsorption of hydroxyurea (HU) on $B_{12}N_{12}$, $CoB_{11}N_{12}$, $FeB_{11}N_{12}$, and $NiB_{11}N_{12}$ nanocages was investigated to identify an efficient drug delivery system. All nanocages exhibited good configurational and chemical stability with physisorption-type interactions. The HU/$NiB_{11}N_{12}$ complex showed the highest stability with adsorption energies of −1.00 eV (gas) and −0.86 eV (water). HU adsorption reduced the HOMO–LUMO energy gap, indicating enhanced electrical conductivity, supported by DOS analysis. Quantum molecular descriptors reveal that $NiB_{11}N_{12}$ possesses low reactivity, high sensitivity, and superior chemical stability. Water-phase results further confirm favorable adsorption and increased polarity. Overall, $NiB_{11}N_{12}$ emerges as the most promising HU drug delivery nanocarrier.

Using DFT in both the gas and water phases, we examined the adsorption nature of the HU drug on $B_{12}N_{12}$, $CoB_{11}N_{12}$, $FeB_{11}N_{12}$, and $NiB_{11}N_{12}$ nanocages to identify the most effective drug delivery vehicle. Our analysis confirms that these nanocages are both configurationally and chemically stable for HU adsorption. Adsorption energy (E_{AD}) calculations revealed that all interactions are of the physisorption type. Among them, the HU/$NiB_{11}N_{12}$ complex exhibited the highest stability, with adsorption energies of −1.00 eV (gas phase) and −0.86 eV (water phase). The HOMO–LUMO energy gap (E_g) decreases as a result of HU adsorption onto these nanocages, suggesting improved electrical conductivity. The drug distribution mechanism depends on the quantity of conduction electrons, which rises when E_g falls. Significant diversity in E_g values across the adsorbents is further confirmed by the DOS study.

The quantum molecular descriptors (QMDs) reveal that the HU/$NiB_{11}N_{12}$ complex demonstrates low reactivity, high sensitivity, and superior chemical stability compared to others. In addition, water-phase calculations highlight the influence of the biological environment, where both DM and E_{AD} values suggest favorable adsorption behavior and enhanced polarity in the complexes. Taken together, these findings indicate that while all the investigated nanocages are effective HU carriers, the $NiB_{11}N_{12}$ nanocage stands out as the most promising drug delivery system due to its superior adsorption behavior, sensitivity, and stability.

Author contributions

Samiron Kumar Saha: writing – original draft, calculations, formal analysis, and resources. Maliha Nishat: formal analysis, writing – review and editing and supervision. Md. Rayhan Mostofa: investigation and data curation. Md. Abul Hasnat: review and editing and visualization. Md. Atikur Rahman: visualization. Md. Hafijur Rahman: visualization.

Conflicts of interest

The authors declare no conflicts of interest.

Data availability

The data will be made available upon request.

Acknowledgements

We are appreciative of the opportunity to use the finely configured computer in the Computational Physics (CP) Research Lab at Pabna University of Science and Technology's Department of Physics. The present investigation forms part of a research project grant facilitated by Pabna University of Science and Technology (PUST), Bangladesh, and the University Grants Commission (UGC).

References

1 K. N. Munny, T. Ahmed, A. A. Piya and S. U. D. Shamim, *Struct. Chem.*, 2023, **34**, 2089–2105.
2 K. Madaan, D. Kaushik and T. A. VerM, *Expert Rev. Anticancer Ther.*, 2012, **12**, 19–29.
3 H. B. Newton, S. R. Scott and C. Volpi, *Br. J. Neurosurg.*, 2004, **18**, 495–499.
4 B. T. Ragel, D. L. Gillespie, V. Kushnir, N. Polevaya, D. Kelly and R. L. Jensen, *Neurosurgery*, 2006, **59**, 1109–1120.
5 E. Mutschler and H. Derendorf, Medpharm Sci. Publ., CRC Press, Stuttgart, 1995, vol. 79, p. 350.
6 W. Y. Gao, A. Cara, R. C. Gallo and F. Lori, *Proc. Natl. Acad. Sci. U. S. A.*, 1993, **90**, 8925–8928.
7 R. Sharon, I. Tatarsky and Y. Ben-Arieh, *Cancer*, 1986, **57**, 718–720.
8 M. López Rubio and M. Argüello Marina, *J. Clin. Med.*, 2024, **13**, 1–15.
9 E. S. Lee, M. M. Heller, F. Kamangar, K. Park, W. Liao and J. Koo, *Psoriasis Forum*, 2011, **17a**, 180–187.
10 C. Besses and A. Alvarez-Larrán, *Clin. Lymphoma, Myeloma Leuk.*, 2016, **16**, S114–S123.
11 F. Quattrone, V. Dini, S. Barbanera, N. Zerbinati and M. Romanelli, *J. Tissue Viability*, 2013, **22**, 112–121.
12 R. E. Ware and B. Aygun, *Am. Soc. Hematol.*, 2009, 62–69.
13 J. T. Chou, W. T. Beck, T. Khwaja, K. Mayer and E. J. Lien, *J. Pharm. Sci.*, 1977, **11**, 1556–1561.
14 M. Chehelgerdi, M. Chehelgerdi, O. Q. B. Allela, R. D. C. Pecho, N. Jayasankar, D. P. Rao, T. Thamaraikani, M. Vasanthan, P. Viktor, N. Lakshmaiya, M. J. Saadh, A. Amajd, M. A. Abo-Zaid, R. Y. Castillo-Acobo, A. H. Ismail, A. H. Amin and R. Akhavan-Sigari, *Mol. Cancer*, 2023, **22**, 1–103.

15 M. Abbasi, E. Nemati-Kande and M. D. Mohammadi, *Comput. Theor. Chem.*, 2018, **1132**, 1–11.
16 M. Rakib Hossain, M. Mehade Hasan, S. Ud Daula Shamim, T. Ferdous, M. Abul Hossain and F. Ahmed, *Comput. Theor. Chem.*, 2021, **1197**, 113156.
17 P. Marbaniang, I. Patil, M. Lokanathan, H. Parse, D. Catherin Sesu, S. Ingavale and B. Kakade, *ACS Sustainable Chem. Eng.*, 2018, **6**, 11115–11122.
18 F. Hui, C. Pan, Y. Shi, Y. Ji, E. Grustan-Gutierrez and M. Lanza, *Microelectron. Eng.*, 2016, **163**, 119–133.
19 Y. Zhang, Z. Xia, Q. Li, G. Gui, G. Zhao, S. Luo, M. Yang and L. Lin, *Int. J. Electrochem. Sci.*, 2018, **13**, 5995–6004.
20 P. Ahmad, M. U. Khandaker, N. Muhammad, F. Rehman, G. Khan, M. A. Rehman, S. M. Ahmed, M. Gulzar, A. Numan and A. S. Khan, *Ceram. Int.*, 2017, **43**, 7358–7361.
21 C. Wang, Y. Long, Y. Deng, Y. Han, D. Tishkevich, M. N. Ha and Q. Weng, *BMEMat*, 2024, **2**, 1–23.
22 H. Zhu, C. Zhao, Q. Cai, X. Fu and F. R. Sheykhahmad, *Inorg. Chem. Commun.*, 2020, **114**, 107808.
23 A. Soltani, A. Sousaraei, M. Bezi Javan, M. Eskandari and H. Balakheyli, *New J. Chem.*, 2016, **40**, 7018–7026.
24 X. Sun, X. Wan, G. Li, J. Yu and V. Vahabi, *Phys. Lett. A*, 2020, **384**, 126128.
25 M. R. Hossain, M. M. Hasan, N. E. Ashrafi, H. Rahman, M. S. Rahman, F. Ahmed, T. Ferdous and M. A. Hossain, *Phys. E*, 2021, **126**, 114483.
26 N. Abdolahi, M. Aghaei, A. Soltani, Z. Azmoodeh, H. Balakheyli and F. Heidari, *Spectrochim. Acta, Part A*, 2018, **204**, 348–353.
27 M. Nishat, M. R. Hossain, M. M. Hasan, M. K. Hossain, M. A. Hossain and F. Ahmed, *J. Biomol. Struct. Dyn.*, 2023, **41**, 3413–3429.
28 S. A. Bithe, M. Hasan, A. A. Oishi, P. Dhali and D. Roy, *Phys. Scr.*, 2023, **98**, 075010.
29 S. Kumar, R. Mostofa, R. Ghosh, F. Ahmad, A. Hasnat, M. Rahman, R. Hossain and M. Nishat, *Comput. Theor. Chem.*, 2024, **1241**, 114873.
30 S. Kumar, M. Nishat, R. Mostofa and A. Hasnat, *Chem. Phys. Lett.*, 2025, **878**, 142332.
31 J. H. Al-Fahemi, K. A. Soliman, S. Eid, E. K. Alenezy, A. H. Naggar, K. S. El-Nasser and S. A. Aal, *J. Inorg. Organomet. Polym. Mater.*, 2025, **36**, 3079–3096.
32 J. P. Perdew, K. Burke and M. Ernzerhof, *Phys. Rev. Lett.*, 1996, **77**, 3865–3868.
33 B. Delley, *Phys. Rev. B:Condens. Matter Mater. Phys.*, 2002, **66**, 1–9.
34 X. Pan, Q. X. Cai, W. L. Chen, G. L. Zhuang, X. N. Li and J. G. Wang, *Comput. Mater. Sci.*, 2013, **67**, 174–181.
35 D. Farmanzadeh and M. Keyhanian, *Theor. Chem. Acc.*, 2019, **138**, 1–10.
36 S. Majedi, F. Behmagham and M. Vakili, *J. Chem. Lett.*, 2020, **1**, 19–24.
37 S. U. D. Shamim, T. Hussain, M. R. Hossian, M. K. Hossain, F. Ahmed, T. Ferdous and M. A. Hossain, *J. Mol. Model.*, 2020, **26**, 1–17.
38 R. Geetha Sadasivan Nair, A. K. Narayanan Nair and S. Sun, *New J. Chem.*, 2024, **48**, 8093–8105.
39 S. Bibi, S. Ur-Rehman, L. Khalid, I. A. Bhatti, H. N. Bhatti, J. Iqbal, F. Q. Bai and H. X. Zhang, *RSC Adv.*, 2022, **12**, 2873–2887.
40 E. U. Ejiofor, J. E. Ishebe, I. Benjamin, G. A. Okon, T. E. Gber and H. Louis, *Heliyon*, 2023, **9**, e20682.
41 A. A. Piya and A. K. M. A. Hossain, *RSC Adv.*, 2023, **13**, 27309–27320.
42 J. Pre-proofs, *Chem. Phys. Lett.*, 2020, 137701.
43 K. Fukui, *Science*, 1982, **218**, 747–754.
44 M. G. Muktadir, A. Alam, A. A. Piya and S. U. D. Shamim, *RSC Adv.*, 2022, **12**, 29569–29584.
45 S. Jameh-Bozorghi and H. Soleymanabadi, *Phys. Lett. A*, 2017, **381**, 646–651.
46 A. Shokuhi Rad and V. Pouralijan Foukolaei, *Synth. Met.*, 2015, **210**, 171–178.
47 M. Souri, *Chem. Phys. Lett.*, 2023, **830**, 140769.
48 G. Job and F. Herrmann, *Eur. J. Phys.*, 2006, **27**, 353–371.
49 N. Islam and D. C. Ghosh, *J. Quantum Inf. Sci.*, 2011, **01**, 135–141.
50 A. Shokuhi Rad, S. Alijantabar Aghouzi, N. Motaghedi, S. Maleki and M. Peyravi, *Mol. Simul.*, 2016, **42**, 1519–1527.
51 C. Xiao, K. Ma, G. Cai, X. Zhang and E. Vessally, *J. Mol. Graphics Modell.*, 2020, **96**, 107539.
52 F. Li, X. Gao, R. Wang, T. Zhang and G. Lu, *Sens. Actuators, B*, 2017, **248**, 812–819.
53 S. N. Ema, M. A. Khaleque, A. Ghosh, A. A. Piya, U. Habiba and S. U. D. Shamim, *RSC Adv.*, 2021, **11**, 36866–36883.